CHAPTER 7

Green synthesis of iron nanoparticles using ayurvedic composition *Triphala* and its constituents for the removal of Cr(VI) and malachite green dye from water

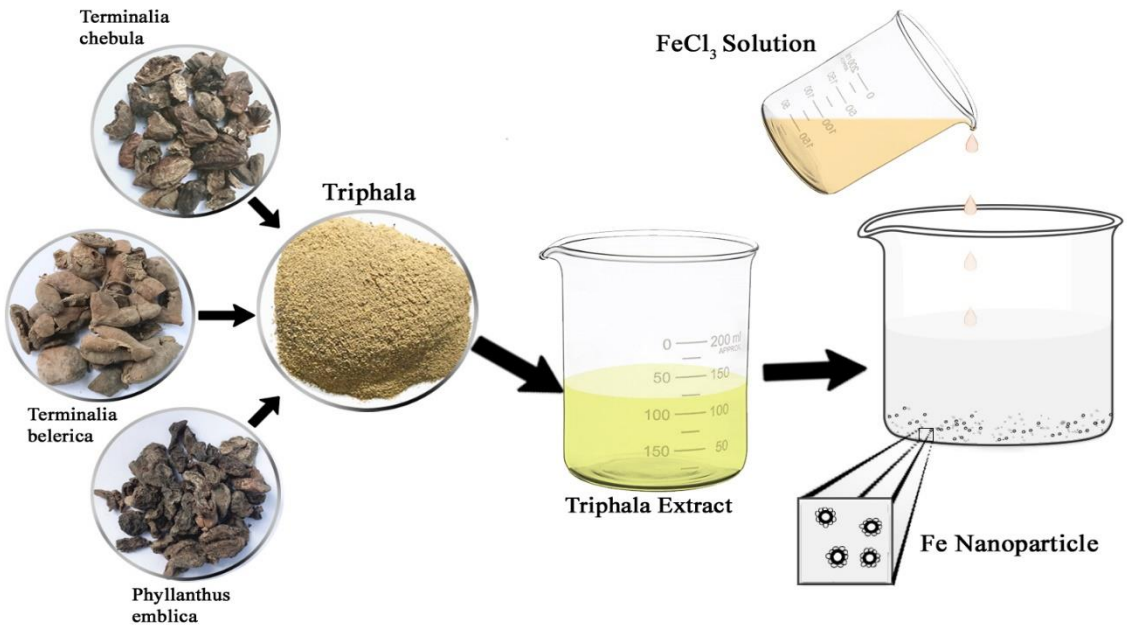

Chapter 7

Green synthesis of iron nanoparticles using ayurvedic composition *Triphala* and its constituents for the removal of Cr(VI) and malachite green dye from water

7.1. Introduction

As discussed in chapter 6, the green synthesis of Fe nanoparticles and their application in water treatment is a vast area of research. The tremendous availability of plant materials always opens up doors for a new horizon. In this study, ayurvedic composition *Triphala* (TP) and its constituents such as *Terminalia chebula* (TC), *Terminalia belerica* (TB) and *Phyllanthus emblica* (PE) have been studied for the preparation of iron nanoparticles. *Triphala* is a powdered preparation of dried fruits of TC, TB and PE in equal proportion. Dried fruit extract of TC contains chebulic acid, theophylline, stigmasterol, brassicasterol[1], gallic acid, protocatechuic acid, catechin, quinic acid, orientin, chlorogenic acid, epicatechin, mangiferin, ferulic acid, sinapic acid, isoorientin, vitexin, chebulinic acid, isovitexin, rutin, ellagic acid, naringin, kaempferol-3-o-rutinoside, eriodictyol, scutellarein, quercetin, genistein, kaempferol, apigenin, betulinic acid, arjunetin, amentoflavone, arjungenin, chrysin and arjunolic acid[2]. Mohan et al. synthesised gold and silver nanoparticles using an aqueous extract of TC seed powder since the phytochemicals present in the TC have the potential to act as reducing and stabilizing agents [3,4]. Similar to TC, the major phytochemicals present in the TB seed extract are gallic acid, protocatechuic acid, catechin, quinic acid, epicatechin, mangiferin, ferulic acid, sinapic acid, isoorientin, chebulinic acid, ellagic acid, naringin, kaempferol-3-o-rutinoside, eriodictyol, scutellarein, genistein, kaempferol, apigenin, arjunetin, arjungenin and vanillic acid[2]. Silver nanoparticles were prepared by Rama et al. using ethanolic TB extract and their photocatalytic and antimicrobial activity were examined. The results show good efficiency for photocatalytic degradation of methylene blue[5]. Another plant material used in this study is the dried fruit of PE, also known as Indian gooseberry. The major active components in PE extract are quinic acid, caffeic acid, gallic acid, gentisic acid-o-hexoside, catechin, brecifolin, ellagic acid, chrysin, methyl gallate, coumaric acid, betulinic acid, oleanolic acid, quercetin, rutin and kaempferol[6]. Recently renuka et al. synthesised silver nanoparticles using PE extract and tested for antimicrobial

activity[7]. Previous studies show that these plant extracts can be used for the synthesis of metal nanoparticles as reductant, antioxidant, capping and stabilizing agent.

As already stated, *Triphala* is a combination of TC, TB and PE plant fruit powders. Figure 7.1 shows the photographs of *Triphala* and its components. In Ayurveda, *Triphala* possesses more activity than its components. The increased activity of TP belongs to the synergetic effect of plant components. The therapeutic use of *Triphala* and its components includes antimicrobial and anti-inflammatory activities, blood purification, remedy for leucorrhea, headache, pneumonia and tuberculosis[8]. To date, there is no report about the synthesis of Fe nanoparticles using *Triphala* as a reducing and stabilizing agent. In this study, Fe nanoparticles have been prepared using *Triphala* and its constituents and a comparative study has been done on the removal of malachite green (MG) dye and Cr(VI) removal using the prepared nanoparticles. MG removal studies have taken place in the presence of H_2O_2 with prepared nanoparticles. The parameters influencing the removal of pollutants such as nanoparticles dosage, initial concentration of the dye, contact time and solution pH were also examined.

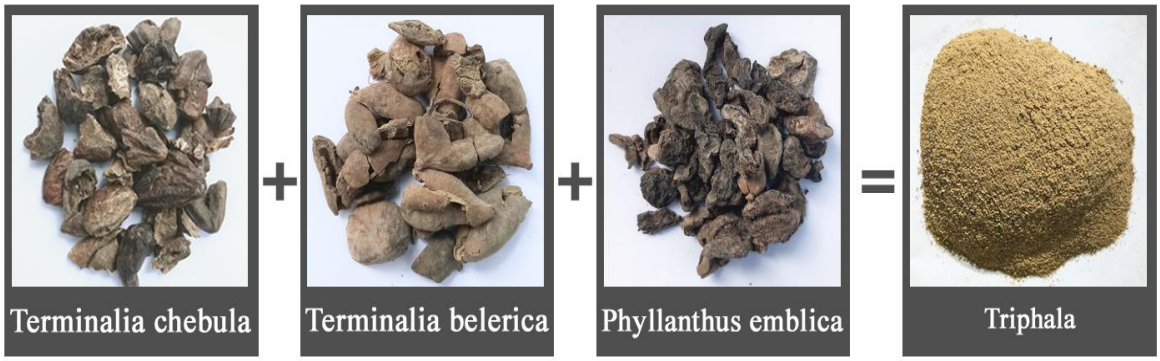

Figure 7.1 *Photographs of Terminalia chebula, Terminalia belerica, Phyllanthus emblica and Triphala*

7.2. Experimental details

7.2.1 Preparation of plant extracts and phytogenic Fe nanoparticles

Preparation of TC, TB, PE and TP extract

To prepare *Triphala* powder, equal amounts of the dried pericarp of three fruits, *Terminalia chebula*, *Terminalia belerica* and *Phyllanthus emblica* were weighed separately and ground to powder. The *Triphala* extracts (20 g/L) were prepared by refluxing 2 g of *Triphala* powder in 100 mL ethanol at a temperature of 90 ºC for 2 hours.

The extract was then cooled, filtered using Whatman number 40 filter paper and stored at 4 ºC for further use.

A similar procedure was followed for the preparation of TC, TB and PE plant extracts. These plant extracts with 20 mg/L concentration were prepared by refluxing 2 g of plant powder in 100 mL ethanol followed by cooling and filtration.

Synthesis of phytogenic Fe nanoparticles

The procedure for synthesising phytogenic Fe nanoparticles was already discussed in chapter 6, except plant extracts used in this study were TP, TC, TB and PE. After the synthesis, the lyophilised nanoparticles were stored for characterisation studies.

7.2.2 Batch experiments

Cr(VI) removal studies

In Cr(VI) removal studies, prepared nanoparticles were used in liquid form. In the optimised condition, 10 mL of 5 mg/L Cr(VI) solution were treated with 0.2 mL of freshly prepared nanoparticles. Different parameters examined in this study were nanoparticle dosage (0.1-0.5 mL), initial concentration of Cr(VI) (1-7 mg/L), initial pH of the solution (4-10) and contact time (10-40 min). NaOH (1.0 M) and H_2SO_4 (1.0 M) were used for the pH adjustment and all the experiments were performed with a duplicate.

Malachite green dye removal studies

The procedure followed for the MG removal studies by phytogenic Fe nanoparticles were also discussed in chapter 6. The different parameters studied to check the efficiency of prepared nanoparticles were nanoparticle dosage (1-5 mL), initial concentration of MG dye (10 - 50 mg/L), pH of the solution (5 - 9) and contact time (10-40 min).

7.2.3 Characterisation and analytical techniques used

The prepared plant extracts were characterised by UV-visible spectrophotometer and GC-MS/MS. The procedure for GC-MS/MS analysis was discussed in chapter 3. The characterisation of nanoparticles have been done using HRTEM, EDAX, FTIR and UV-visible spectrophotometer and the details of characterisation techniques are discussed in chapter 2. Fourier transform infrared spectra of the prepared plant extracts and corresponding Fe nanoparticles were investigated through Spectrum Two Fourier

transform infrared spectrometer (FTIR, Perkin Elmer, USA). Jeol 6390LA/OXFORD XMX N was used for the elemental analysis of TC-Fe, TB-Fe, PE-Fe and TP-Fe nanoparticles.

7.3. Results and discussion

7.3.1 Characterisation of TP plant extract

No.	Retention time (t)	Name of the compound	Molecular weight	Action	Reference
a.	13.47	5-(hydroxymethyl)furan-2-carbaldehyde	126	Reducing agent	[9]
b.	16.37	benzene-1,3,5-triol	126	Reducing and capping agent	[10]
c.	16.57	benzene-1,2,3-triol	126	Reducing and capping agent	[10]
d.	17.25	2,2,4-trimethyl-1H-quinoline	173	Antioxidant	[11]
e.	18.09	2,6-ditert-butyl-4-methylphenol	220	Reducing agent and antioxidant	[12]
f.	19.71	4,7-dimethoxy-5-prop-2-enyl-1,3-benzodioxole	222	Antioxidant	[13]
g.	20.42	3H-1,3-benzothiazol-2-one	151	Antioxidant	[14]
h.	23.16	methyl hexadecanoate	270	Antioxidant	[15]
i.	23.49	hexadecanoic acid	256	Antioxidant and stabilizing agent	[16,17]
j.	23.85	ethyl hexadecanoate	284	Antioxidant	[15]

Table 7.1 *Biomolecules identified in TP extract by GC-MS/MS*

The phytochemical analysis of ethanolic TP plant extract was done using GC-MS/MS and identified ten bioactive compounds. The results show that TP extract contains reducing, stabilizing and antioxidizing agents. Retention time, molecular weight and mode of action of the bioactive compounds are presented in table 7.1. In the extract, the presence of methyl hexadecanoate/ethyl hexadecanoate may be due to the esterification of hexadecenoic acid with ethanol, which is used as a solvent for the extraction of plant components. Recently Hao et al. synthesised Fe nanoparticles from green tea aqueous extract and confirmed that the presence of bioactive components like benzene-1,3,5-triol and benzene-1,2,3-triol acted as reducing and capping agents during Fe nanoparticles formation[10]. Mass spectra of the identified bioactive components have been shown in figure 7.2.

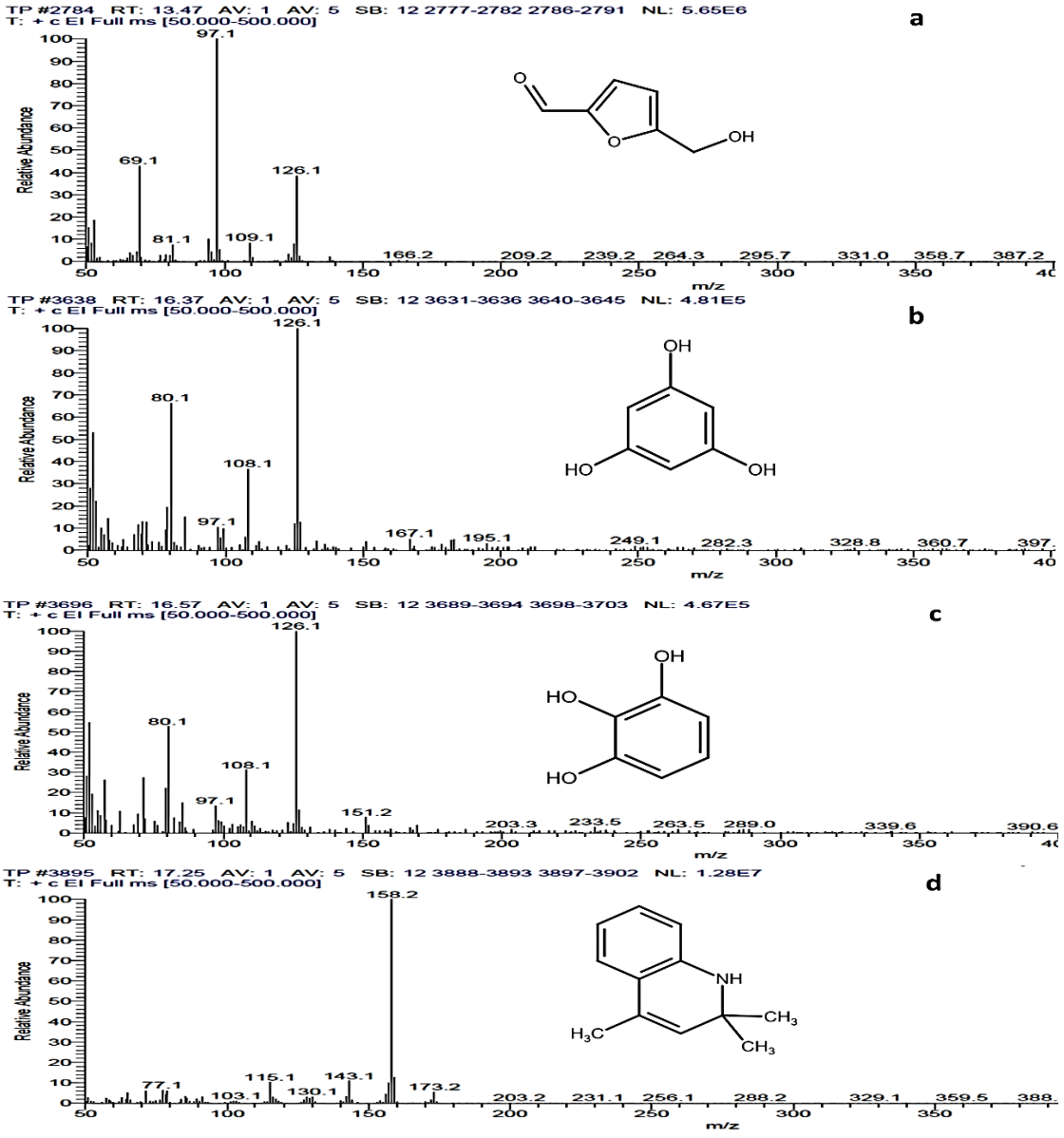

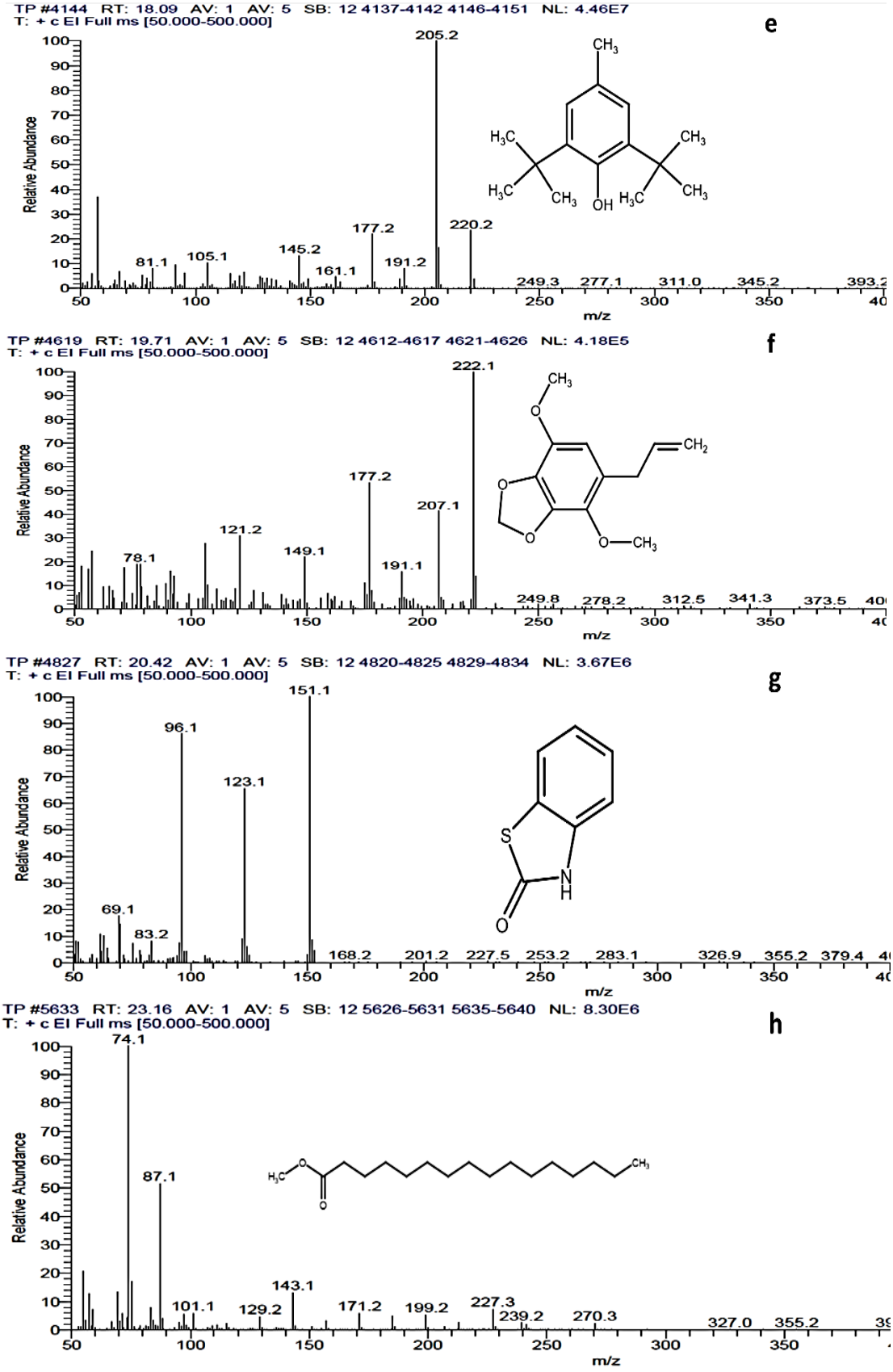
TP #4144 RT: 18.09 AV: 1 AV: 5 SB: 12 4137-4142 4146-4151 NL: 4.46E7
T: + c EI Full ms [50.000-500.000]
e
205.2
177.2
220.2
145.2
81.1
105.1
161.1
191.2
249.3
277.1
311.0
345.2
Relative Abundance
m/z
TP #4619 RT: 19.71 AV: 1 AV: 5 SB: 12 4612-4617 4621-4626 NL: 4.18E5
T: + c EI Full ms [50.000-500.000]
f
222.1
177.2
207.1
121.2
149.1
78.1
191.1
249.8
278.2
312.5
341.3
373.5
Relative Abundance
m/z
TP #4827 RT: 20.42 AV: 1 AV: 5 SB: 12 4820-4825 4829-4834 NL: 3.67E6
T: + c EI Full ms [50.000-500.000]
g
151.1
96.1
123.1
69.1
83.2
168.2
201.2
227.5
253.2
283.1
326.9
355.2
379.4
Relative Abundance
m/z
TP #5633 RT: 23.16 AV: 1 AV: 5 SB: 12 5626-5631 5635-5640 NL: 8.30E6
T: + c EI Full ms [50.000-500.000]
h
74.1
87.1
143.1
101.1
129.2
171.2
199.2
227.3
239.2
270.3
327.0
355.2
Relative Abundance
m/z

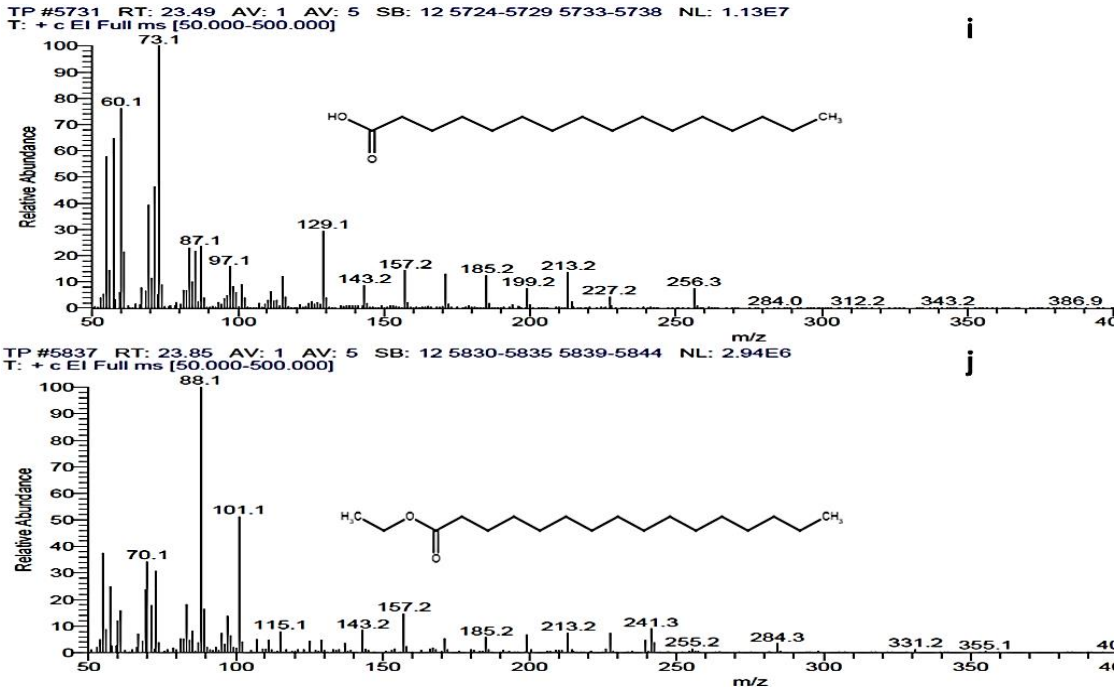

Figure 7.2 *Mass spectra of compounds identified in TP extract by GC-MS/MS. (a) 5-(hydroxymethyl)furan-2-carbaldehyde; (b) benzene-1,3,5-triol; (c) benzene-1,2,3-triol; (d) 2,2,4-trimethyl-1H-quinoline; (e) 2,6-ditert-butyl-4-methylphenol; (f) 4,7-dimethoxy-5-prop-2-enyl-1,3-benzodioxole; (g) 3H-1,3-benzothiazol-2-one; (h) methyl hexadecanoate; (i) hexadecanoic acid; (j) ethyl hexadecanoate*

7.3.2 Characterisation of TC-Fe, TB-Fe, PE-Fe and TP-Fe nanoparticles

UV-visible spectroscopy

As discussed in chapter 6, the development of black precipitate during the mixing of iron salt solution and plant extract indicates the formation of Fe nanoparticles[18]. Figure 7.3 shows the photographs and UV-visible spectra of plant extracts before and after reaction with the iron salt solution. The broad peak centred around 600 nm indicates the formation of Fe nanoparticles. However, the plant extracts and Fe salt solution does not exhibit any transition in this region[19].

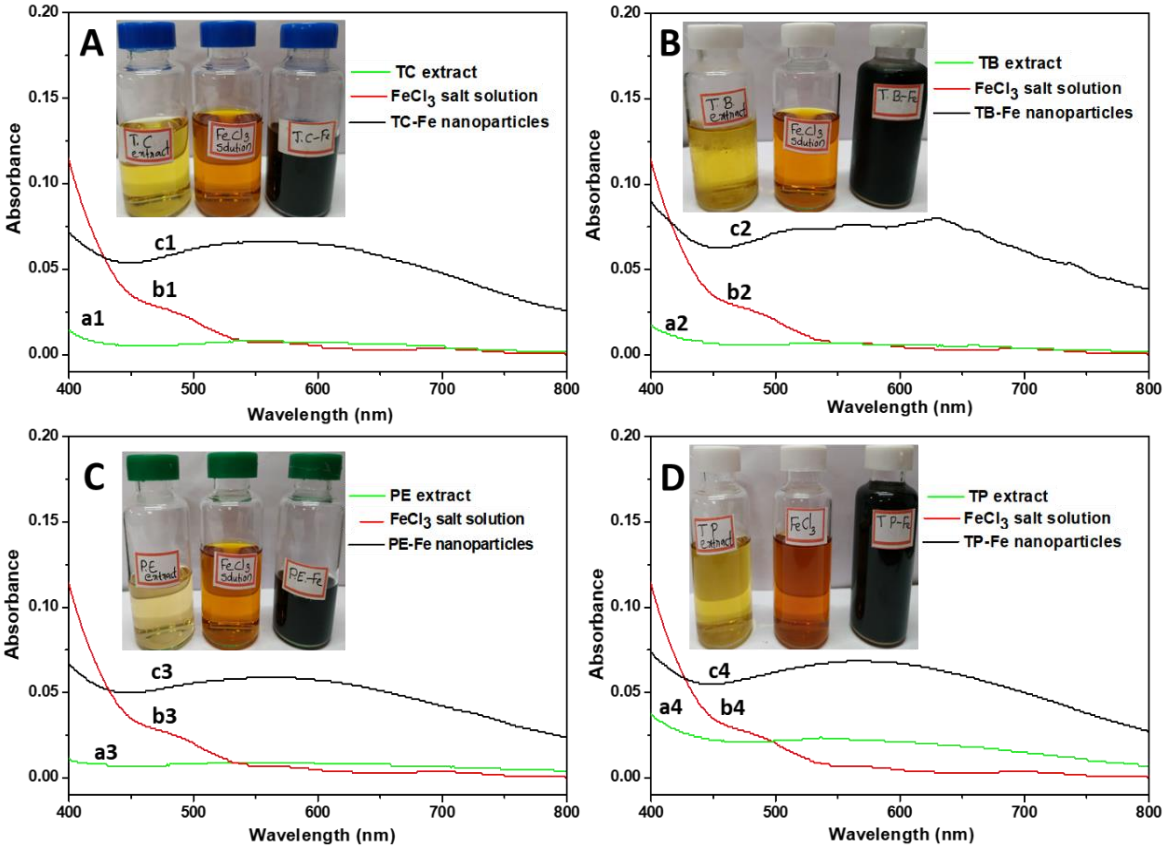

Figure 7.3 *Photographs and UV-visible spectra of A) a1. TC extract, b1. $FeCl_3$ solution and c1. TC-Fe nanoparticles, B) a2. TB extract, b2. $FeCl_3$ solution and c2. TB-Fe nanoparticles, C) a3. PE extract, b3. $FeCl_3$ solution and c3. PE-Fe nanoparticles, D) a4. TP extract, b4. $FeCl_3$ solution and c4. TP-Fe nanoparticles*

HRTEM

Figure 7.4 shows the HRTEM images and SAED pattern of TC-Fe, TB-Fe and PE-Fe nanoparticles. Figure 7.4 (a, b, & c) envisages that the formed Fe nanoparticles are covered with plant materials and agglomerated as a chain/needle-like structure. The formation of nanoparticles is more evident from figure 7.4 (a1, b1 & c1) and it indicates that the formed nanoparticles have a particle size below 6 nm. The TC-Fe, TB-Fe and PE-Fe nanoparticles have an average particle size of 5.2, 2.4 and 3 nm respectively and the d-spacing of the Fe nanoparticles is observable. TC-Fe nanoparticles show a d-spacing of 2.7 Å, which corresponds to the (220) plane of Fe_3O_4[20]. However, TB-Fe and PE-Fe nanoparticles showed a d-spacing of 2.6 Å and this corresponds to the (311) plane of Fe_3O_4[21]. SAED pattern of all the three iron oxide nanoparticles (figure 7.4) show only diffused rings and no bright spots which indicates the amorphous nature of the TC-Fe, TB-Fe and PE-Fe nanoparticles.

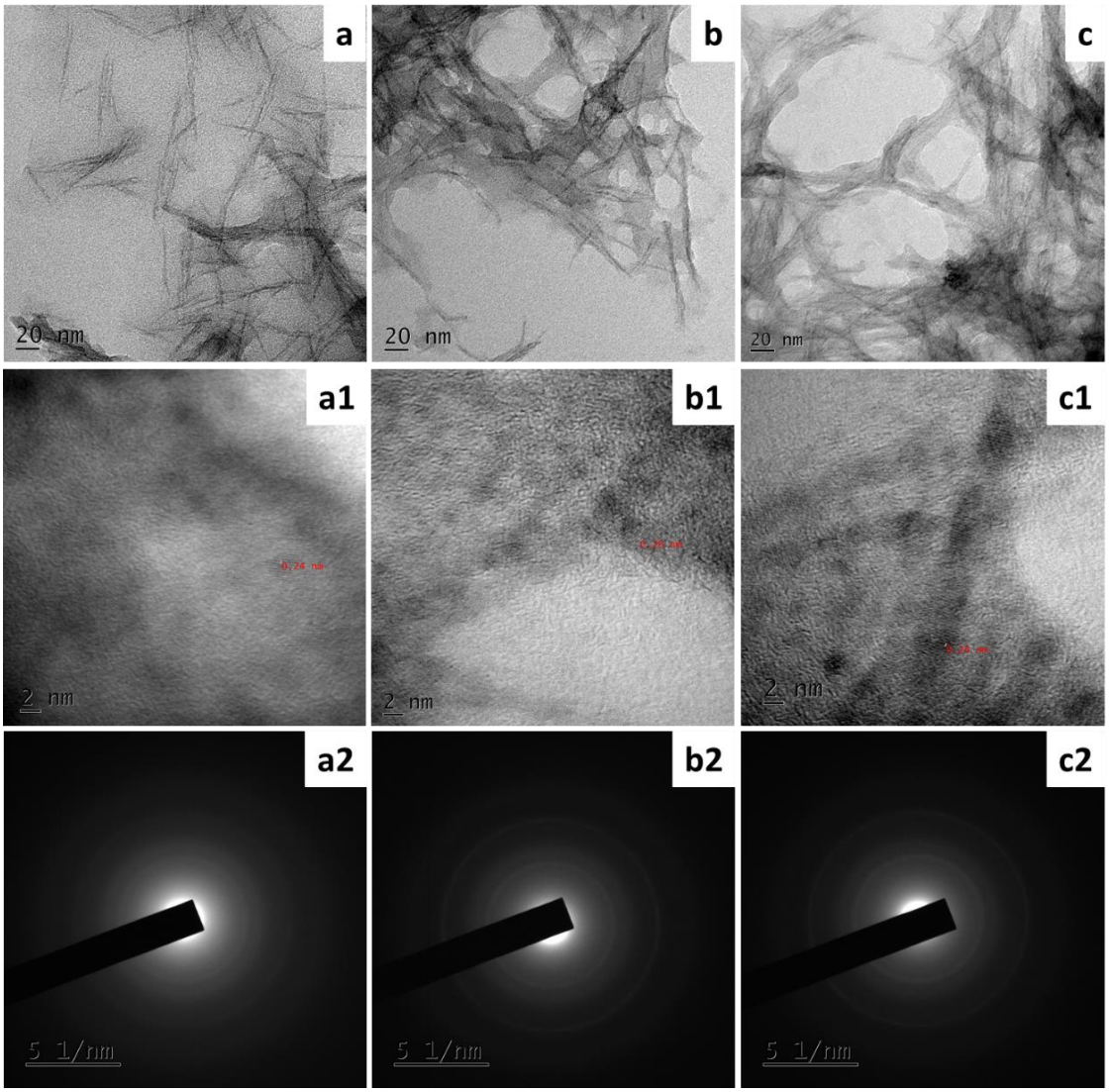

Figure 7.4 *HRTEM image of the (a-a1) TC-Fe, (b-b1) TB-Fe and (c-c1) PE-Fe nanoparticles and SAED pattern of (a2) TC-Fe, (b2) TB-Fe and (c2) PE-Fe nanoparticles*

Figure 7.5 (a & a1) displays the HRTEM image and SAED pattern of the TP-Fe nanoparticles. As shown in figure 7.5a, irregularly shaped nanoparticles were agglomerated and unevenly dispersed in the plant extract. The size of the TP-Fe nanoparticles was varied from 7-14 nm with an average diameter of 11 nm. SAED pattern displays faded spots with diffused rings, indicating the presence of crystalline and amorphous Fe particles in TP-Fe. The d-spacing values calculated from the SAED pattern of TP-Fe are 2.01 Å and 1.29 Å which corresponds to the (110) plane of Fe^0[22] and (311) plane of FeO (JCPDS No 00-006-0615). The formation of and Fe^0 and FeO nanoparticles suggest that the synergetic effect of three plant components improved the reduction and

stabilization potential of TP extract and the growth of the nanoparticles was also enhanced significantly.

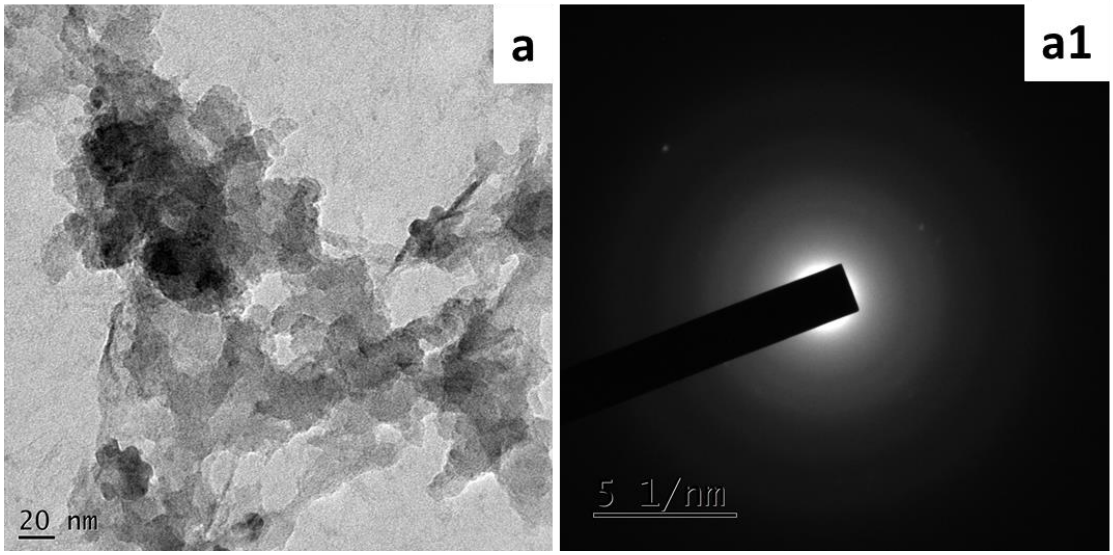

Figure 7.5 *(a) HRTEM image and (a1) SAED pattern of the TP-Fe nanoparticles*

EDAX

Figure 7.6 demonstrates the EDAX spectra of the TC-Fe, TB-Fe, PE-Fe and TP-Fe nanoparticles. The results reveal that the atomic percentage of Fe in TC-Fe, TB-Fe, PE-Fe and TP-Fe nanoparticles were 6.33, 8.01, 8.60 and 6.62 % respectively. The other elements such as C from plant components, Cl from $FeCl_3$ and O by air oxidation were also present in the prepared nanoparticles.

Figure 7.7 shows the EDAX mapping (Fe and O mapping images) of TC-Fe, TB-Fe, PE-Fe and TP-Fe nanoparticles. EDAX mapping of the prepared nanoparticles inferred that Fe is uniformly and finely distributed in TC-Fe, TB-Fe and PE-Fe nanoparticles however in the case of TP-Fe nanoparticles, more aggregation of Fe can be seen in the Fe mapping image. This agrees with the HRTEM results in which more coarse particles were identified. The presence of oxygen in the prepared nanoparticles may be from the iron oxide and the plant components adsorbed on the nanoparticles.

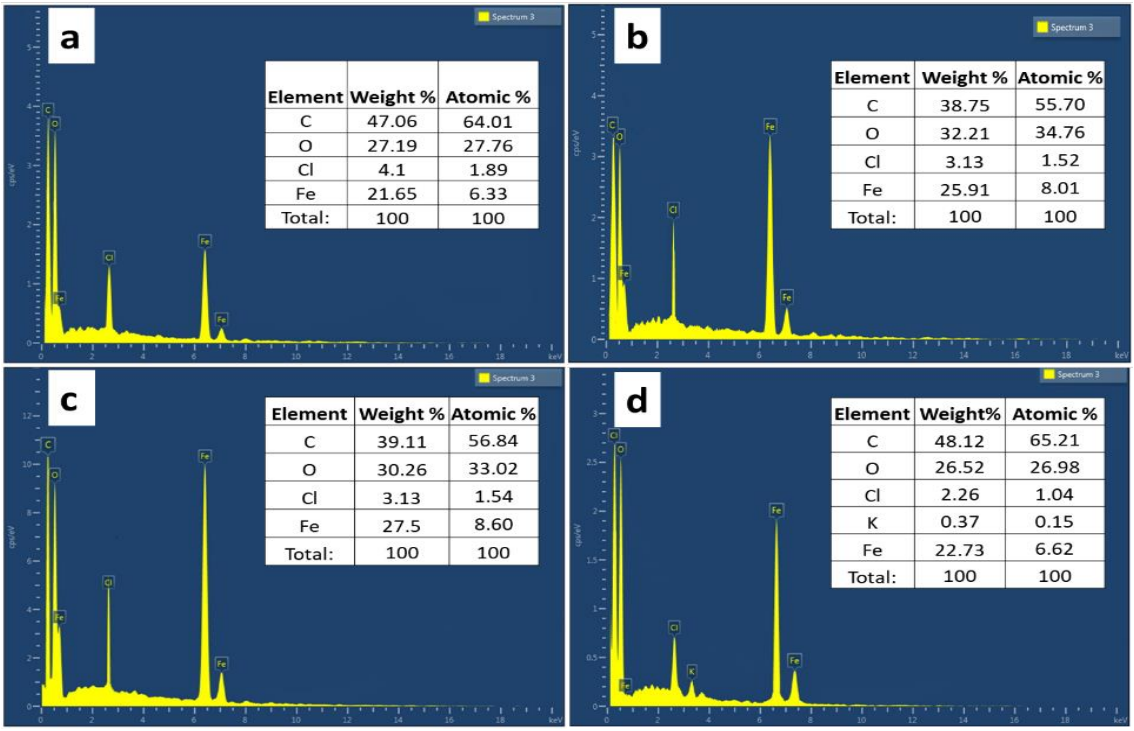

Figure 7.6 *EDAX spectra of a) TC-Fe, b) TB-Fe, c) PE-Fe and d) TP-Fe nanoparticles*

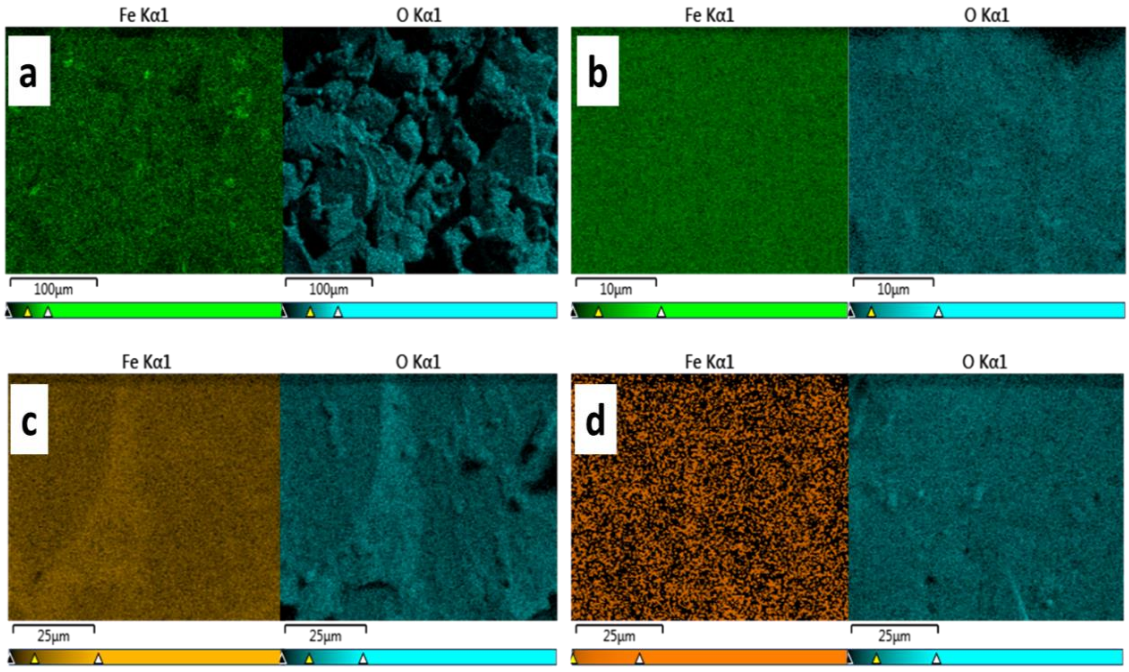

Figure 7.7 *EDAX mapping of a) TC-Fe, b) TB-Fe, c) PE-Fe and d) TP-Fe nanoparticles*

FTIR spectroscopy

The FTIR spectra of TC, TB, PE and TP plant extracts and their corresponding Fe nanoparticles are shown in figure 7.8(a, b, c & d). All the plant extracts show characteristic peaks of almost similar functional groups. Similar to AP-Fe and SN-Fe nanoparticles

discussed in chapter 6, a broad peak is seen between 3700-3000 cm^{-1} in all the plant extracts and in Fe nanoparticles which corresponds to the O-H and N-H stretching vibrations of the polyphenols and amines present[23]. The groups present in the prepared plant extracts based on the FTIR results were O-H, N-H, C-H, C=O, C=C, C-N, C-Br and C-I, which is due to the presence of polyphenols, carboxylic acids, amino acids and alkaloids in them. Most of the functional groups can also be seen in the corresponding Fe nanoparticles. This indicates that biomolecules in the plant extract are adsorbed on the surface of Fe nanoparticles as a capping/stabilizing agent. However, the FTIR spectra of prepared nanoparticles show some changes in the characteristic peaks. The intensity of certain peaks was increased/decreased whereas some were shifted to higher/lower wavenumbers.

In TP-Fe nanoparticles, the O-H, N-H, C=O, C-N and C-O vibrations were shifted to lower wavenumbers compared to plant extract. For example, 1737 cm^{-1}, 1645 cm^{-1} and 1217 cm^{-1} peaks in TP extract shifted to 1703 cm^{-1}, 1621 cm^{-1} and 1190 cm^{-1}. This may be due to the decreased bond strength of functional groups due to the enhanced interaction with Fe nanoparticles. The peak at 458 cm^{-1} indicates the stretching vibration of Fe-O in the TP-Fe nanoparticles[24]. TC-Fe, TB-Fe and PE-Fe nanoparticles exhibit a different pattern of changes than TP-Fe nanoparticles. In TC-Fe nanoparticles, stretching vibrations of C-N and C=O correspondingly shifted to higher wavenumbers, from 1705 cm^{-1} to 1738 cm^{-1} and 1323 cm^{-1} to 1365 cm^{-1} respectively and vibrations corresponding to C-O changes to lower wavenumber compared to TC extract. Peak shift indicates that these functional groups are involved in the binding mechanism of Fe nanoparticles[25]. In TB-Fe nanoparticles, O-H, N-H, C=O, C-N and C=C characteristic peaks were shifted to higher wavenumbers, whereas in PE-Fe nanoparticles, C=C, O-H and N-H peaks were shifted to higher wavenumber compared to respective plant extracts. Changes in FTIR spectra indicate that reduction and stabilization of these Fe nanoparticles proceeded via these functional groups. The FTIR spectra of the prepared plant extracts and the respective Fe nanoparticles confirmed that the plant biocomponents synergistically employ reducing and capping/stabilizing properties during the synthesis of Fe nanoparticles.

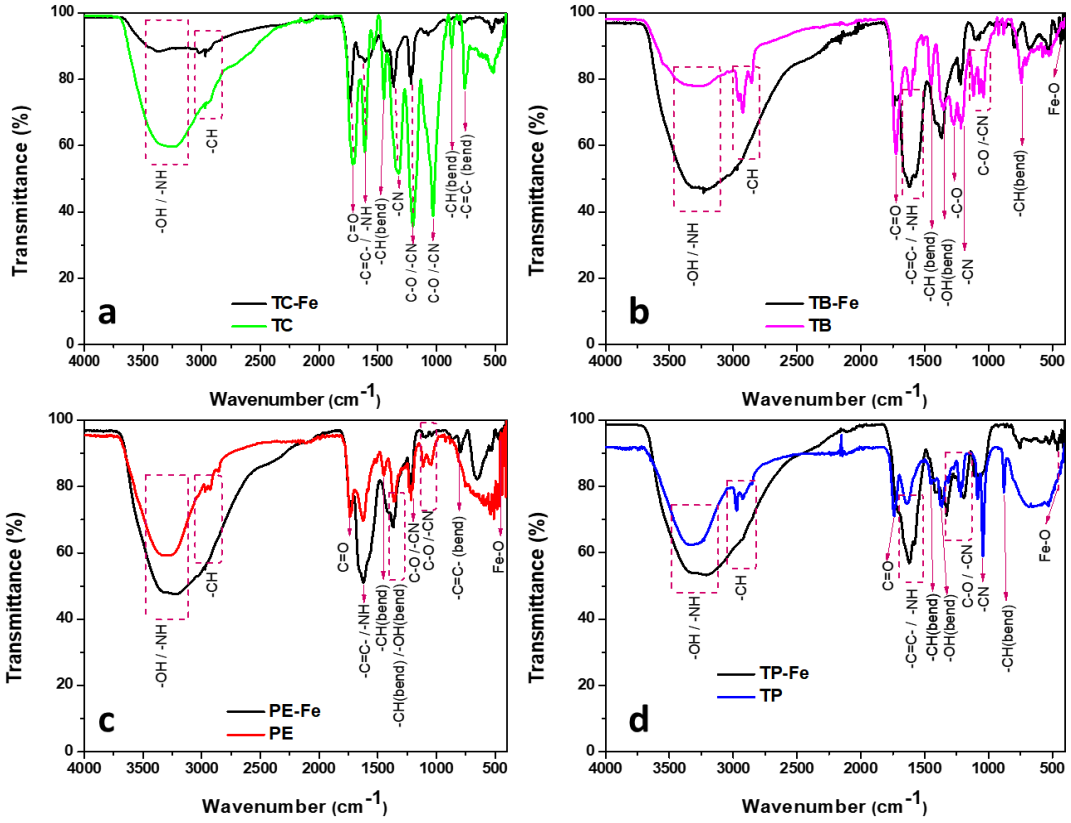

Figure 7.8 *FTIR spectra of a) TC-Fe, b) TB-Fe, c) PE-Fe and d) TP-Fe nanoparticles*

7.3.3 Cr(VI) removal studies

Figure 7.9 shows the Cr(VI) removal efficiency of TC-Fe, TB-Fe, PE-Fe and TP-Fe nanoparticles studied using 0.2 mL phytogenic nanoparticles added to 10 mL Cr(VI) solution having 5 mg/L concentration for 15 minutes. TP-Fe nanoparticles show the highest Cr(VI) removal efficiency in the prepared nanoparticles followed by TC-Fe, PE-Fe and TB-Fe nanoparticles. This may be due to the compositional difference of the Fe nanoparticles since TP-Fe contains Fe^0 and FeO nanoparticles whereas TC-Fe, PE-Fe and TB-Fe have Fe_3O_4 composition[26]. As discussed in chapter 6 the reduction, precipitation and adsorption are the pathway mechanisms followed for removing Cr(VI) using phytogenic Fe nanoparticles[27,28]. Along with the Fe nanoparticles, the capped plant components also have some ability to remove Cr(VI) from water. For example, Gajanan et al. removed Cr(VI) from water using *Terminalia chebula*[29]. The synergistic effect of plant components and Fe nanoparticles drastically improved the Cr(VI) removal efficiency. The effect of different parameters such as nanoparticle dosage, initial

concentration of Cr(VI), initial pH of the Cr(VI) solution and contact time were investigated for Cr(VI) removal.

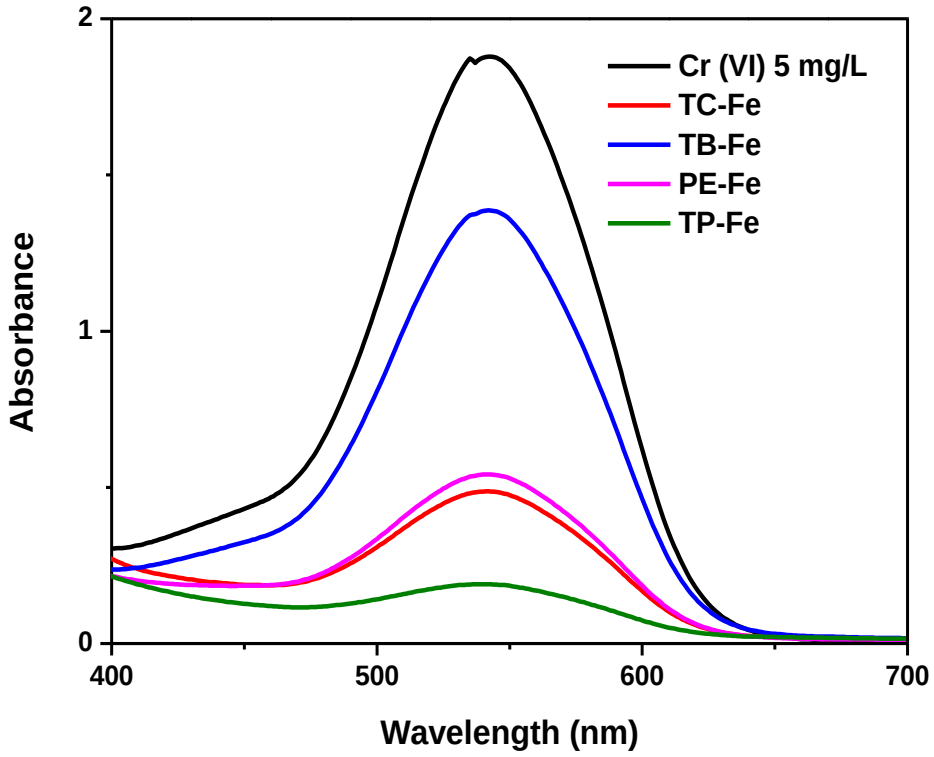

Figure 7.9 *UV-visible spectra of Cr(VI) solution after treating with nanoparticles*

Effect of nanoparticle dosage

As expected, the Cr(VI) removal efficiency increased with increasing nanoparticles dosage from 0.1 mL to 0.5 mL maintaining the initial Cr(VI) concentration (5 mg/L) and contact time (15 min) kept constant. This is simply because of increased effective active sites in the system with nanoparticle dosage. As shown in figure 7.10a, the highest removal efficiency has been shown by TP-Fe nanoparticles. PE-Fe and TC-Fe nanoparticles have almost similar removal efficiency and the lowest removal efficiency has been shown by TB-Fe nanoparticles. At 0.4 mL nanoparticles dosage, all the prepared nanoparticles except TB-Fe showed almost 100 % removal efficiency.

Effect of the initial concentration of the Cr(VI) solution

The effect of initial Cr(VI) concentration on the Cr(VI) removal was documented in figure 7.10b. The nanoparticles dosage (0.2 mL) and contact time (15 minutes) were kept

constant throughout the study. As the concentration increases from 1 to 7 mg/L, the percentage of Cr(VI) removal efficiency decreases in all the prepared Fe nanoparticles. This is due to the unvarying available surface active sites at constant nanoparticle dosage required for complete Cr(VI) removal at higher concentrations. In 3 mg/L Cr(VI) solution, the TC-Fe, TB-Fe, PE-Fe and TP-Fe nanoparticles show 88.9 %, 37.6 %, 89.2 % and 100 % of Cr(VI) removal efficiency respectively.

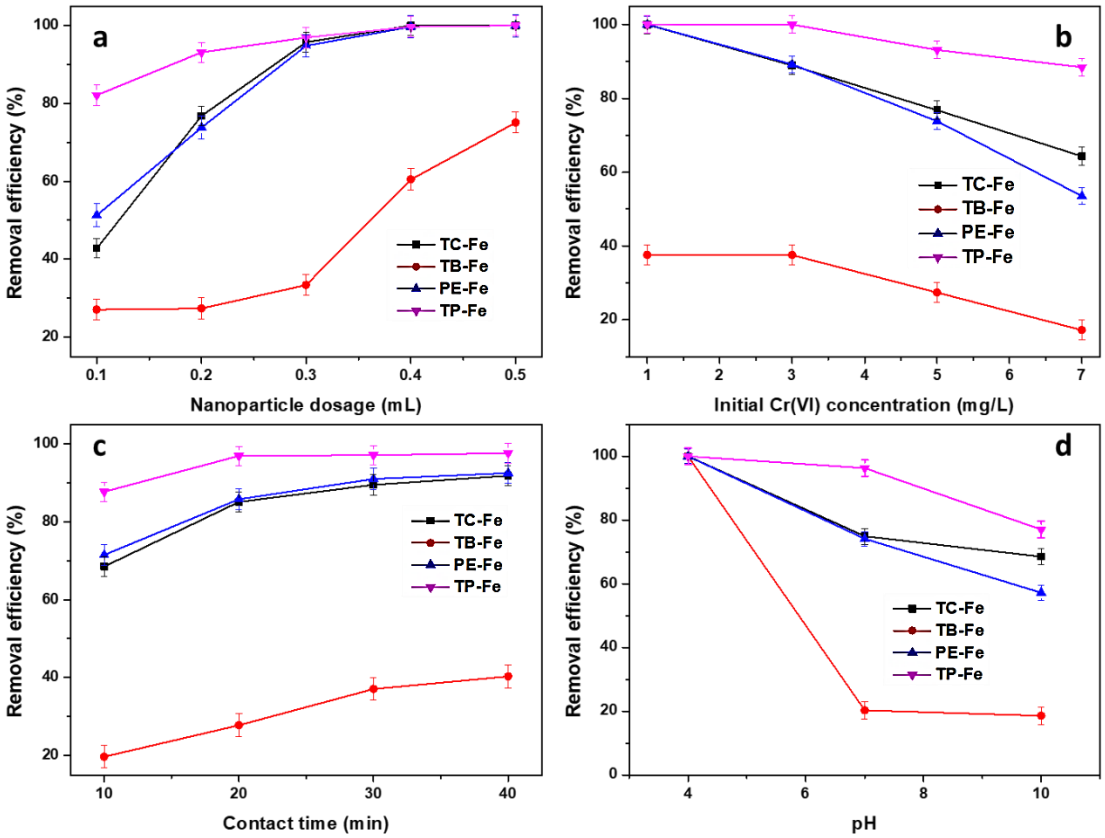

Figure 7.10 *Effects of various factors on Cr(VI) removal: (a) nanoparticle dosage, (b) initial Cr(VI) concentration, (c) contact time and (d) initial solution pH .*

Effect of contact time

Figure 7.10c represents the study of the effect of contact time in TC-Fe, TB-Fe, PE-Fe and TP-Fe nanoparticles while keeping all other parameters constant. As expected, Cr(VI) removal efficiency increases with increasing contact time since more contact time results more interaction between Fe nanoparticles and Cr(VI) in solution. In TP-Fe nanoparticles, there is no significant changes in Cr(VI) removal after 10 minutes which indicates that the removal process by TP-Fe nanoparticles appears very fast. On the other hand,

nanoparticles such as TC-Fe, TB-Fe and PE-Fe attained plateau in Cr(VI) removal after 30 minutes only.

Effect of pH

As discussed in chapter 3, the pH of the solution significantly influences the Cr(VI) removal efficiency. Figure 7.10d represents the effect of solution pH in Cr(VI) removal keeping all other parameters constant. At pH 4, all the nanoparticles show 100 % removal efficiency, which is drastically reduced into 68 %, 18 %, 57 % and 77 % in TC-Fe, TB-Fe, PE-Fe and TP-Fe nanoparticles respectively, at pH 10. This may be due to the fact that in acidic pH, the positively charged surface of Fe nanoparticles attracts the negatively charged Cr(VI) ions, improving the removal efficiency[19].

7.3.4 MG dye removal studies

The prepared TC-Fe, TB-Fe, PE-Fe and TP-Fe nanoparticles were evaluated by examining their ability to remove MG dye. The prepared nanoparticles were used as heterogeneous Fenton-like catalysts in the presence of H_2O_2. Applying a heterogeneous Fenton-like system in dye removal is attractive since it causes the complete mineralisation of dye molecules and retard the formation of slurry, which is usually seen in a homogeneous Fenton system[30]. Figure 7.11 represents the MG removal using prepared nanoparticles and H_2O_2. The results show that TP-Fe nanoparticles have the highest removal efficiency, followed by PE-Fe, TB-Fe and TC-Fe nanoparticles. H_2O_2 alone does not show significant removal efficiency compared to Fe nanoparticles. The mechanism for MG removal was similar to AP-Fe and SN-Fe nanoparticles discussed in chapter 6. Adsorption of MG into iron oxide and degradation through the ·OH radicals results in the removal of MG dye molecules[31]. TP-Fe nanoparticles show the highest removal efficiency since they are mainly composed of Fe^0 and FeO compared to other nanoparticles composed of Fe_3O_4 and Fe_3O_4.

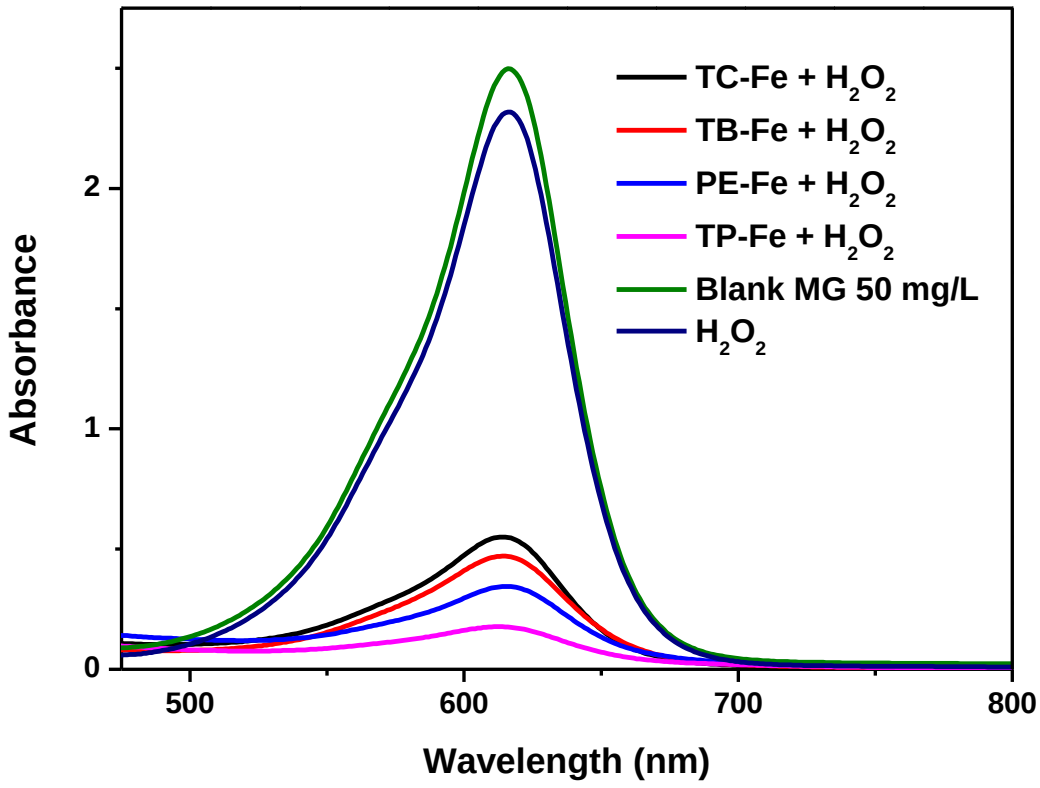

Figure 7.11 *UV-visible spectra of MG dye solution after treating with nanoparticles*

Effect of nanoparticle dosage

It is not surprising that MG dye removal increases with increasing nanoparticles dosage. The availability of more Fe nanoparticles for adsorption and Fenton reaction results in improved MG dye removal at higher nanoparticles dosage. Figure 7.12a represents the MG removal by phytogenic nanoparticles with varying nanoparticle dosages from 0.5 mL to 2.5 mL while keeping the initial dye concentration (50 mg/L) and contact time (15 min) constant. At 1 mL nanoparticle dosage, 76 %, 82 %, 86 % and 93 % removal efficiency were shown by TC-Fe, TB-Fe, PE-Fe and TP-Fe nanoparticles respectively. As expected, the removal efficiency increases with increasing nanoparticle dosage.

Effect of initial concentration of the MG

Figure 7.12b represents the effect of the initial concentration of MG on the removal of MG dye molecules, keeping nanoparticle dosage (1 mL) and contact time (15 min) constant. The removal efficiency decreases slightly with an increase in the initial concentration of the MG dye. This is because of the insufficient availability of Fe nanoparticles corresponding to the increased concentration of MG dye. The highest removal efficiency

was seen in the solution of 10 mg/L and the increasing order of removal efficiency was 89 %, 92 %, 94 % and 98 % for TC-Fe, TB-Fe, PE-Fe and TP-Fe nanoparticles.

Effect of contact time

The effect of contact time on MG removal efficiency was studied and represented in figure 7.12c. The nanoparticle dosage (1 mL) and initial concentration of MG dye (50 mg/L) were kept constant during the study. In the first 10 minutes, TC-Fe, TB-Fe, PE-Fe and TP-Fe nanoparticles showed 71 %, 84 %, 90 % and 90 % removal efficiency, respectively. When it was increased to 40 minutes, the removal efficiency was 75 %, 87 %, 95 % and 95 %. The results show that the removal efficiency increases with increasing contact time; however, the rate of increase is not much significant.

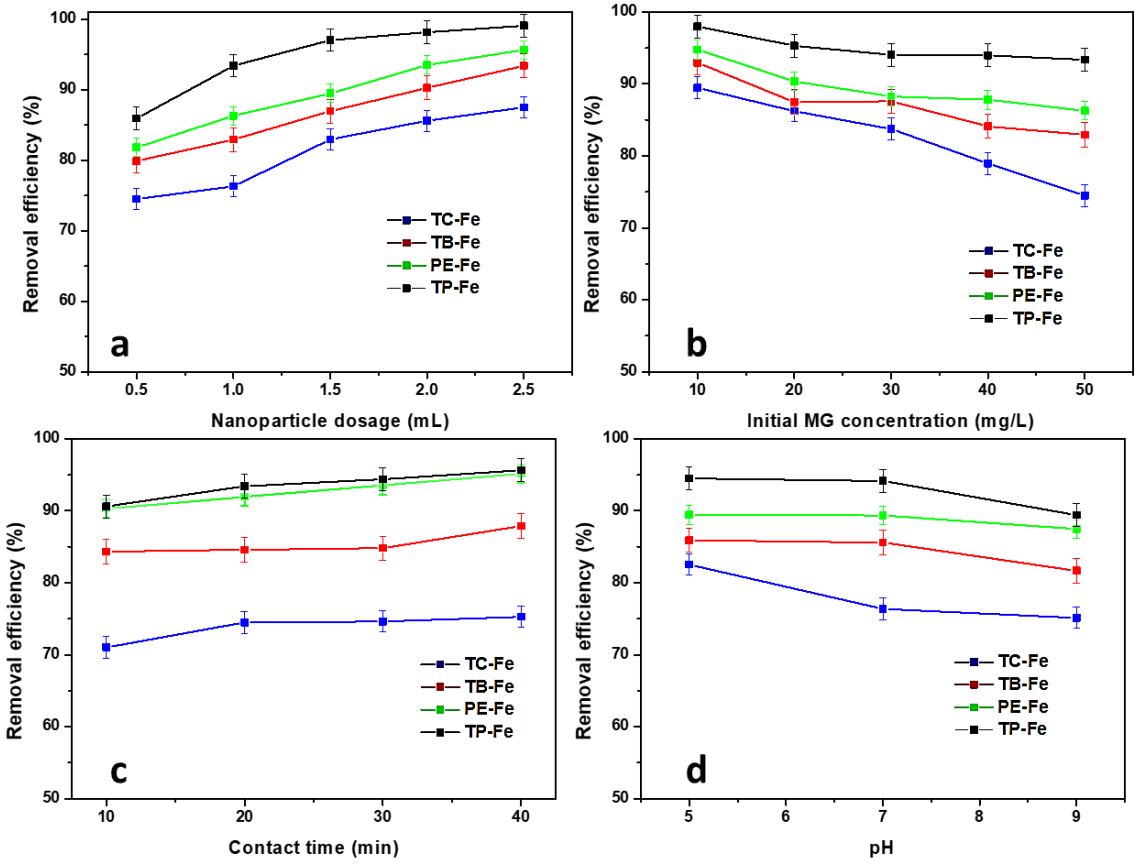

Figure 7.12 *Effects of various factors on MG removal (a) nanoparticle dosage, (b) initial MG concentration, (c) contact time and (d) initial solution pH.*

Effect of pH

The effect of pH on the removal of MG dye was illustrated in figure 7.12d. The TC-Fe, TB-Fe, PE-Fe and TP-Fe nanoparticles show 76 %, 85 %, 89 % and 94 % removal efficiency at neutral pH. However, the removal efficiency decreases slightly when it shifts to basic pH. This is due to the formation of ferric/ferrous hydroxide complexes. Acidic pH improves the removal efficiency of the prepared nanoparticles.

7.4. Conclusions

In summary, phytogenic Fe nanoparticles were synthesised using ayurvedic composition *Triphala* and its constituents such as *Terminalia chebula, Terminalia belerica* and *Phyllanthus emblica*. The characterization of nanoparticles was done by UV-visible spectroscopy, HRTEM, EDAX and FTIR. The appearance of the broad band around 600 nm suggests the formation of Fe nanoparticles in the solution. HRTEM results suggest that the nanoparticles have a particle size less than 6 nm when using plant extracts. However, the particles size of *Triphala* based Fe nanoparticles was around 11 nm. The SAED pattern indicates that the composition of prepared nanoparticles mainly consists of iron oxides. FTIR confirmed the presence of organic components in the prepared nanoparticles that might induce stability to the prepared nanoparticles. The application of prepared nanoparticles for Cr(VI) removal studies clearly indicates that TP-Fe nanoparticles have the highest removal efficiency, followed by TC-Fe, PE-Fe and TB-Fe nanoparticles. However, in the case of MG dye removal, again the TP-Fe nanoparticles have the highest removal efficiency followed by PE-Fe, TB-Fe and TC-Fe nanoparticles.

7.5. References

[1] G. Subramanian, D. Shanmugamprema, R. Subramani, K. Muthuswamy, V. Ponnusamy, K. Tankay, T. Velusamy, V. Krishnan, S. Subramaniam, Anti-Obesity Effect of T. Chebula Fruit Extract on High Fat Diet Induced Obese Mice: A Possible Alternative Therapy, Mol. Nutr. Food Res. 65 (2021) 2001224. https://doi.org/10.1002/mnfr.202001224.

[2] A. Singh, V. Bajpai, S. Kumar, B. Kumar, M. Srivastava, K.B. Rameshkumar, Comparative profiling of phenolic compounds from different plant parts of six Terminalia species by liquid chromatography–tandem mass spectrometry with chemometric analysis, Ind. Crops Prod. 87 (2016) 236–246. https://doi.org/10.1016/j.indcrop.2016.04.048.

[3] K. Mohan Kumar, B.K. Mandal, M. Sinha, V. Krishnakumar, Terminalia chebula mediated green and rapid synthesis of gold nanoparticles, Spectrochim. Acta Part A Mol. Biomol. Spectrosc. 86 (2012) 490–494. https://doi.org/10.1016/j.saa.2011.11.001.

[4] K. Mohan Kumar, M. Sinha, B.K. Mandal, A.R. Ghosh, K. Siva Kumar, P. Sreedhara Reddy, Green synthesis of silver nanoparticles using Terminalia chebula extract at room

temperature and their antimicrobial studies, Spectrochim. Acta Part A Mol. Biomol. Spectrosc. 91 (2012) 228–233. https://doi.org/10.1016/j.saa.2012.02.001.

[5] R. Sharma, Synthesis of Terminalia bellirica fruit extract mediated silver nanoparticles and application in photocatalytic degradation of wastewater from textile industries, Mater. Today Proc. 44 (2021) 1995–1998. https://doi.org/10.1016/j.matpr.2020.12.118.

[6] S. Kumar, A. Singh, B. Kumar, Identification and characterization of phenolics and terpenoids from ethanolic extracts of Phyllanthus species by HPLC-ESI-QTOF-MS/MS, J. Pharm. Anal. 7 (2017) 214–222. https://doi.org/10.1016/j.jpha.2017.01.005.

[7] R. Renuka, K.R. Devi, M. Sivakami, T. Thilagavathi, R. Uthrakumar, K. Kaviyarasu, Biosynthesis of silver nanoparticles using phyllanthus emblica fruit extract for antimicrobial application, Biocatal. Agric. Biotechnol. 24 (2020) 101567. https://doi.org/10.1016/j.bcab.2020.101567.

[8] S. Ranjani, K. Tamanna, S. Hemalatha, Triphala green nano colloids: synthesis, characterization and screening biomarkers, Appl. Nanosci. 10 (2020) 1269–1279. https://doi.org/10.1007/s13204-019-01208-w.

[9] W. Liang, R. Zhu, X. Li, J. Deng, Y. Fu, Heterogeneous photocatalyzed acceptorless dehydrogenation of 5-hydroxymethylfurfural upon visible-light illumination, Green Chem. 23 (2021) 6604–6613. https://doi.org/10.1039/D1GC01286J.

[10] R. Hao, D. Li, J. Zhang, T. Jiao, Green Synthesis of Iron Nanoparticles Using Green Tea and Its Removal of Hexavalent Chromium, Nanomaterials. 11 (2021) 650. https://doi.org/10.3390/nano11030650.

[11] B. Ibrahim, A. Wiranata, A. Malik, The Effect of Addition of Antioxidant 1,2-dihydro-2,2,4-trimethyl-quinoline on Characteristics of Crepe Rubber Modified Asphalt in Short Term Aging and Long Term Aging Conditions, Appl. Sci. 10 (2020) 7236. https://doi.org/10.3390/app10207236.

[12] M.Z. Kassaee, M. Mohammadkhani, A. Akhavan, R. Mohammadi, In situ formation of silver nanoparticles in PMMA via reduction of silver ions by butylated hydroxytoluene, Struct. Chem. 22 (2011) 11–15. https://doi.org/10.1007/s11224-010-9671-1.

[13] M.M. Saleh-e-In, N. Sultana, M.M. Rahim, M.A. Ahsan, M.N.H. Bhuiyan, M.N. Hossain, M.M. Rahman, S. Kumar Roy, M.R. Islam, Chemical composition and pharmacological significance of Anethum Sowa L. Root, BMC Complement. Altern. Med. 17 (2017) 127. https://doi.org/10.1186/s12906-017-1601-y.

[14] H. Chabane, M. Messarah, M. Liacha, Comparative study for the synthesis of new generation of2(3H)-benzothiazolones as antioxidant agents, Der Pharma Chem. 8 (2016) 20–26.

[15] T. Sudha, S. Chidambarampillai, V.. Mohan, GC-MS analysis of bioactive components of aerial parts of fluggea leucopyrus willd. (Euphorbiaceae), J. Appl. Pharm. Sci. 3 (2013) 126–130. https://doi.org/10.7324/JAPS.2013.3524.

[16] P. Bhuyar, M.H.A. Rahim, S. Sundararaju, R. Ramaraj, G.P. Maniam, N. Govindan, Synthesis of silver nanoparticles using marine macroalgae Padina sp. and its antibacterial activity towards pathogenic bacteria, Beni-Suef Univ. J. Basic Appl. Sci. 9 (2020) 3. https://doi.org/10.1186/s43088-019-0031-y.

[17] S. Siswadi, G.S. Saragih, Phytochemical analysis of bioactive compounds in ethanolic extract of Sterculia quadrifida R.Br., in: 2021: p. 030098. https://doi.org/10.1063/5.0053057.

[18] A. Rana, N. Kumari, M. Tyagi, S. Jagadevan, Leaf-extract mediated zero-valent iron for oxidation of Arsenic (III): Preparation, characterization and kinetics, Chem. Eng. J. 347 (2018) 91–100. https://doi.org/10.1016/j.cej.2018.04.075.

[19] Z. Xiao, H. Zhang, Y. Xu, M. Yuan, X. Jing, J. Huang, Q. Li, D. Sun, Ultra-efficient removal of chromium from aqueous medium by biogenic iron based nanoparticles, Sep. Purif. Technol. 174 (2017) 466–473. https://doi.org/10.1016/j.seppur.2016.10.047.

[20] D. Patiño-Ruiz, L. Sánchez-Botero, L. Tejeda-Benitez, J. Hinestroza, A. Herrera, Green synthesis of iron oxide nanoparticles using Cymbopogon citratus extract and sodium carbonate salt: Nanotoxicological considerations for potential environmental applications, Environ. Nanotechnology, Monit. Manag. 14 (2020) 100377. https://doi.org/10.1016/j.enmm.2020.100377.

[21] T. Sarkar, T.K. Dhiman, R.K. Sajwan, S. Sri, P.R. Solanki, Studies on carbon-quantum-dot-embedded iron oxide nanoparticles and their electrochemical response, Nanotechnology. 31 (2020) 355502. https://doi.org/10.1088/1361-6528/ab925e.

[22] W. Teng, J. Fan, W. Wang, N. Bai, R. Liu, Y. Liu, Y. Deng, B. Kong, J. Yang, D. Zhao, W. Zhang, Nanoscale zero-valent iron in mesoporous carbon (nZVI@C): stable nanoparticles for metal extraction and catalysis, J. Mater. Chem. A. 5 (2017) 4478–4485. https://doi.org/10.1039/C6TA10007D.

[23] K.V.G. Ravikumar, S.V. Sudakaran, K. Ravichandran, M. Pulimi, C. Natarajan, A. Mukherjee, Green synthesis of NiFe nano particles using Punica granatum peel extract for tetracycline removal, J. Clean. Prod. 210 (2019) 767–776. https://doi.org/10.1016/j.jclepro.2018.11.108.

[24] S. Eslami, M.A. Ebrahimzadeh, P. Biparva, Green synthesis of safe zero valent iron nanoparticles by: Myrtus communis leaf extract as an effective agent for reducing excessive iron in iron-overloaded mice, a thalassemia model, RSC Adv. 8 (2018) 26144–26155. https://doi.org/10.1039/c8ra04451a.

[25] W.K.A. Wan Mat Khalir, K. Shameli, S.D. Jazayeri, N.A. Othman, N.W. Che Jusoh, N.M. Hassan, Biosynthesized Silver Nanoparticles by Aqueous Stem Extract of Entada spiralis and Screening of Their Biomedical Activity, Front. Chem. 8 (2020). https://doi.org/10.3389/fchem.2020.00620.

[26] Y. Wei, Z. Fang, L. Zheng, E.P. Tsang, Biosynthesized iron nanoparticles in aqueous extracts of Eichhornia crassipes and its mechanism in the hexavalent chromium removal, Appl. Surf. Sci. 399 (2017) 322–329. https://doi.org/10.1016/j.apsusc.2016.12.090.

[27] F. Zhu, S. He, T. Liu, Effect of pH, temperature and co-existing anions on the Removal of Cr(VI) in groundwater by green synthesized nZVI/Ni, Ecotoxicol. Environ. Saf. 163 (2018) 544–550. https://doi.org/10.1016/j.ecoenv.2018.07.082.

[28] F. Zhu, S. Ma, T. Liu, X. Deng, Green synthesis of nano zero-valent iron/Cu by green tea to remove hexavalent chromium from groundwater, J. Clean. Prod. 174 (2018) 184–190. https://doi.org/10.1016/j.jclepro.2017.10.302.

[29] G. Kapure, S. Mohan Rao, Application of Terminalia chebula for Removal of Hexavalent Chromium in Chromite Concentrates, ISIJ Int. 48 (2008) 868–874. https://doi.org/10.2355/isijinternational.48.868.

[30] S.S.F. Carvalho, N.M.F. Carvalho, Dye degradation by green heterogeneous Fenton catalysts prepared in presence of Camellia sinensis, J. Environ. Manage. 187 (2017) 82–88. https://doi.org/https://doi.org/10.1016/j.jenvman.2016.11.032.

[31] X. Wang, A. Wang, J. Ma, M. Fu, Facile green synthesis of functional nanoscale zero-valent iron and studies of its activity toward ultrasound-enhanced decolorization of cationic dyes, Chemosphere. 166 (2017) 80–88. https://doi.org/10.1016/j.chemosphere.2016.09.056.